European Journal of Pharmaceutics and Biopharmaceutics 142 (2019) 38–48

Contents lists available at ScienceDirect

European Journal of Pharmaceutics and Biopharmaceutics

journal homepage: www.elsevier.com/locate/ejpb

Research paper

Lipidoid-polymer hybrid nanoparticles loaded with TNF siRNA suppress inflammation after intra-articular administration in a murine experimental arthritis model

Manon A.A. Jansen[a,1], Lasse H. Klausen[b,1], Kaushik Thanki[c], Jeppe Lyngsø[b,d], Jan Skov Pedersen[b,d], Henrik Franzyk[e], Hanne M. Nielsen[c], Willem van Eden[a], Mingdong Dong[b], Femke Broere[a,f], Camilla Foged[c,*], Xianghui Zeng[c,*]

[a] Department of Infectious Diseases and Immunology, Faculty of Veterinary Medicine, Utrecht University, Utrecht, the Netherlands
[b] Interdisciplinary Nanoscience Center, Aarhus University, Gustav Wieds Vej 14, DK-8000 Aarhus C, Denmark
[c] Department of Pharmacy, Faculty of Health and Medical Sciences, University of Copenhagen, Universitetsparken 2, DK-2100 Copenhagen Ø, Denmark
[d] Department of Chemistry, Aarhus University, Gustav Wieds Vej 14, DK-8000 Aarhus C, Denmark
[e] Department of Drug Design and Pharmacology, Faculty of Health and Medical Sciences, University of Copenhagen, Jagtvej 162, DK-2100 Copenhagen Ø, Denmark
[f] Department of Clinical Sciences of Companion Animals, Faculty Veterinary Medicine, Utrecht University, Utrecht, the Netherlands

ARTICLE INFO

Keywords:
Nanoparticles
siRNA delivery
Lipidoid
Vesicles
Macrophage
Arthritis

ABSTRACT

Rheumatoid arthritis (RA) is a common autoimmune disease, which is characterized by painful chronic inflammation in the joints, and novel safe and efficacious treatments are urgently needed. RNA interference (RNAi) therapy based on small interfering RNA (siRNA) is a promising approach for silencing specific genes involved in inflammation. However, delivery of siRNA to the target site, i.e. the cytosol of immune cells, is a challenge. Here, we designed lipid-polymer hybrid nanoparticles (LPNs) composed of lipidoid and poly(DL-lactic-co-glycolic acid) loaded with a therapeutic cargo siRNA directed against the proinflammatory cytokine tumor necrosis factor (TNF), which plays a key role in the progression of RA. We compared their efficacy and safety with reference lipidoid-based stable nucleic acid lipid particles (SNALPs) *in vitro* and *in vivo*. Cryogenic transmission electron microscopy, atomic force microscopy and small-angle X-ray scattering revealed that the mode of loading of siRNA in lamellar structures differs between the two formulations. Thus, siRNA was tightly packed in LPNs, while LPNs displayed lower adhesion than SNALPs. The LPNs mediated a higher TNF silencing effect *in vitro* than SNALPs in the RAW 264.7 macrophage cell line activated with lipopolysaccharide. For both types of delivery systems, macropinocytosis was involved in cellular uptake. In addition, clathrin-mediated endocytosis contributed to uptake of SNALPs. LPNs loaded with TNF siRNA mediated sequence-specific suppression of inflammation in a murine experimental arthritis model upon intra-articular administration. Hence, the present study demonstrates that LPN-mediated TNF knockdown constitutes a promising approach for arthritis therapy of TNF-mediated chronic inflammatory conditions.

1. Introduction

Rheumatoid arthritis (RA) is an autoimmune disease characterized by chronic synovial inflammation, leading to cartilage and bone destruction in the joints [1]. In RA, the regulation of the inflammatory process is deficient, and immune responses against self-antigens are triggered. Currently, medication is directed towards relief of symptoms by the use of disease-modifying anti-rheumatic drugs (DMARDs). These drugs target the immune inflammatory response in a non-specific way, and undesired side effects are frequently experienced by RA patients. Hence, there is a need for novel and more specific treatments, which are efficacious and safe. The pro-inflammatory cytokine tumor necrosis factor (TNF), which is produced by monocytes and macrophages among other cell types, plays a key role in the progression of a wide variety of chronic inflammatory disorders, *e.g.*, RA. It is found in high concentrations in the serum and synovial fluid of patients with RA [2]. TNF does not only induce other pro-inflammatory cytokines, but also the secretion of matrix-degrading proteases produced by fibroblasts,

* Corresponding authors.
E-mail addresses: camilla.foged@sund.ku.dk (C. Foged), zengxh@ynu.edu.cn (X. Zeng).
[1] These authors contributed equally

https://doi.org/10.1016/j.ejpb.2019.06.009
Received 5 November 2018; Received in revised form 17 April 2019; Accepted 10 June 2019
Available online 11 June 2019
0939-6411/

eventually resulting in destruction of cartilage. Currently, patients with RA are treated with anti-TNF biopharmaceuticals, which consist of monoclonal anti-TNF antibodies and soluble TNF receptors. Infliximab (monoclonal TNF antibody) and etanercept (soluble TNF receptor) are the most commonly used anti-TNF biopharmaceuticals. In combination with methotrexate, they are relatively efficacious in inducing disease remission [3,4]. However, one of the disadvantages of this treatment strategy is that infliximab and etanercept may induce antibodies, which can result in response failure [5]. RNA interference (RNAi) therapy can be used to suppress disease-associated exacerbated inflammation and inhibiting TNF overexpression with small interfering RNA (siRNA) can prevent the problem of antibody formation.

However, a drug delivery system is needed to deliver siRNA intracellularly to target the RNAi pathway in the cytosol, because siRNA cannot permeate cellular membranes. A vast number of different cationic lipids and helper lipids have been intensively studied for delivery of exogenous nucleic acids into cells [6]. Cationic lipids form lipoplexes with nucleic acids by complexation with polyanionic nucleic acids via attractive electrostatic interactions. Owing to their fusogenic properties and ability to undergo structural changes from bilayer to hexagonal structures, certain cationic lipids or helper lipids can improve the transfection efficiency [6]. However, lipoplexes are highly unstable in serum-containing physiological media, eventually resulting in poor *in vivo* performance [7].

A solution to this problem is to combine a polymeric core with a cationic lipid shell layer to form colloidally more stable lipid-polymer hybrid nanoparticles (LPNs) for nucleic acid delivery [8]. We have demonstrated that LPNs composed of poly(DL-lactic-co-glycolic acid) (PLGA) and the cationic lipid 1,2-dioleoyl-3-trimethylammonium propane (DOTAP) efficiently deliver siRNA to cells and mediate high transfection efficiency [9,10]. However, a main challenge is the toxicity of many cationic lipids. Therefore, replacement of the toxicity-associated cationic lipids with alternative and more transfection-competent lipids as the lipid component of LPNs might enable more efficient gene silencing. This would allow for dose reduction, thus improving the overall safety and efficacy of the delivery system. The so-called lipidoids are examples of such compounds that constitute a novel class of lipid-like components based on an alkylated tetraamine backbone [11]. Depending on the alkylation degree, different subtypes are obtained *e.g.*, the penta-substituted lipidoid (i.e. L_5, which appears as an isomeric mixture) and the *hexa*-substituted lipidoid (*i.e.* L_6 being a single fully alkylated entity) [11,12]. We recently showed that if siRNA is encapsulated in LPNs based on PLGA and lipidoids, the intracellular delivery of siRNA is enhanced [12,13]. In contrast to commonly used cationic lipids like DOTAP, lipidoids contain several secondary and tertiary amines, rendering them more efficient in interacting with siRNA without significantly increasing the net charge of the delivery system. Therefore, the siRNA loading is enhanced and the effective dose of cationic lipid needed in lipidoid-LPNs is much lower than that of DOTAP-LPNs at equimolar siRNA concentrations, thereby reducing the side effects. Nevertheless, it is of major concern that bulk lipidoids are able to activate Toll-like receptor (TLR) 4 [13]. However, inclusion of lipidoid into the LPNs structure was shown to abrogate TLR4 activation *in vitro* [13].

To date, we have limited knowledge about the capability of lipidoid-based LPNs to deliver a therapeutic siRNA cargo and ensuing transfection efficiency *in vitro* and *in vivo*. Hence, we investigated the potential of LPNs for intracellular delivery of TNF siRNA resulting in TNF silencing in the murine macrophage cell line RAW 264.7 activated with lipopolysaccharide (LPS). For comparison, we prepared and characterized a reference formulation of TNF siRNA-loaded stable nucleic acid lipid particles (SNALPs) using lipidoid as the cationic lipid component, and investigated how the particle structure and surface properties of these two systems differentially affected the siRNA delivery to activated macrophages *in vitro*. Furthermore, their therapeutic capacities were tested *in vivo* in a murine experimental arthritis model.

2. Materials and methods

2.1. Materials

L_5 was synthesized, purified and characterized as previously reported [11,12]. 2′-O-methyl modified dicer substrate asymmetric siRNA duplexes directed against TNF (TNF siRNA), negative control siRNA and Alexa647-labeled siRNA were kindly provided by GlaxoSmithKline (Stevenage, UK) as dried, purified, and desalted duplexes (Supplementary data, Table S1). Primers were purchased from TAG Copenhagen (Frederiksberg, Denmark). PLGA (lactide:glycolide molar ratio 75:25, Mw: 20 kDa) was purchased from Wako Pure Chemical Industries (Osaka, Japan). Polyvinylalcohol (PVA) 403 with an 80.0% degree of hydrolysis was provided by Kuraray (Osaka, Japan). Cholesterol and C_{16} PEG_{2000} ceramide were purchased from Avanti Polar Lipids (Alabaster, AL, USA). Quant-iT™ RiboGreen® RNA Reagent and Tris–EDTA buffer (10 mM Tris, 1 mM EDTA, pH 7.5) were acquired from Molecular Probes Invitrogen (Paisley, UK). RNase-free diethyl pyrocarbonate (DEPC)-treated Milli-Q water was used for all buffers and dilutions. Additional chemicals were obtained commercially at analytical grade (Sigma-Aldrich, St Louis, MO, USA).

2.2. Preparation and physicochemical characterization of LPNs and SNALPs

The PLGA nanoparticles (NPs), the non-loaded LPNs, and the siRNA-loaded LPNs were prepared using a double emulsion solvent evaporation method as previously reported [12,14]. Briefly, a volume of 125 μL of Tris-EDTA buffer or 66.7 mM TNF siRNA solution (w_1) was emulsified in 250 μL of a 15 mg PLGA in CH_2Cl_2 or 2.25 mg lipidoid/12.75 mg PLGA binary mixture in CH_2Cl_2 (o) by sonication to form a primary emulsion, which was dispersed in 2% (w/v) PVA aqueous solution (w_2), resulting in the formation of a water-in-oil-in-water ($w_1/o/w_2$) double emulsion. With the evaporation of CH_2Cl_2, the emulsion droplets were gradually solidified as LPNs. The LPNs were washed and freeze-dried as previously reported. L_5-based SNALPs loaded with TNF siRNA were prepared using the ethanol destabilization method as previously reported [11,12]. For the Alexa647-labeled particles, TNF siRNA was replaced with the corresponding Alexa647-labeled siRNA.

The intensity-weighted average hydrodynamic diameter (*z*-average) and polydispersity index (PDI) of the NPs were determined by DLS using the photon correlation spectroscopy technique as previously described [12]. Laser-Doppler electrophoresis was used to determine the zeta-potential of the NPs as previously described [12]. The RiboGreen® RNA reagent was used to determine the siRNA encapsulation efficiency and practical loading as previously described [9].

2.3. Cryo-transmission electron microscopy (cryo-TEM)

Morphological analysis was carried out by cryo-TEM using a Tecnai G2 20 TWIN transmission electron microscope (FEI, Hillsboro, OR, USA) as previously described [9]. In brief, samples for cryo-TEM were prepared using a FEI Vitrobot Mark IV. A small droplet was deposited onto a Pelco Lacey carbon-filmed grid and spread carefully; excess liquid was removed, resulting in the formation of a thin sample film. The samples were immediately plunged into liquid ethane and kept at −180 °C. The vitrified samples were subsequently transferred in liquid nitrogen to an Oxford CT3500 cryo holder connected to the electron microscope. The sample temperature was continuously kept below −180 °C. All observations were made in bright field mode at an acceleration voltage of 120 kV. Digital images were recorded with a Gatan Imaging Filter 100 CCD camera (Gatan, Pleasanton, CA, USA).

2.4. Atomic force microscopy (AFM)

LPN dispersions were added to freshly cleaved muscovite mica and

air-dried before characterization using a MultiMode 8 microscope (Bruker, Santa Barbara, CA, USA) operated in PeakForce QNM mode. TAP525A probes (nominal spring constant 200 N/m, nominal tip radius 8 nm) and TAP150 (nominal spring constant 5 N/m, nominal tip radius 8 nm) (Bruker AFM Probes, Camarillo, CA, USA) were calibrated before and after characterization of each sample using an absolute method. Full force distance data was acquired and post processed using the Nano Scope Analysis v 1.80 (Santa Barbara, CA, USA). A nominal force of 100 nN was applied to indent the sample and the Young's Modulus was determined using the Hertz indentation model, while the maximum step height between the baseline and the minimum value of the curve was used to determine adhesion [15].

2.5. Small-angle X-ray scattering (SAXS)

SAXS data were recorded using a modified flux-optimized NanoSTAR SAXS instrument (Bruker AXS) with a rotating Cu source ($\lambda = 1.54$Å) [16], a two-pinhole setup with a home-built scatterless slit/pinhole in front of the sample, a semi-transparent beamstop, and a thermostated sample cell (Anton Paar, Graz, Austria). A home-built flow-through quartz capillary sample cell ($\varnothing = 2$mm) was used for the measurements. Data were recorded with a VÅNTEC-500 2D-area detector (Bruker AXS). LPNs (10 mg/mL) or SNALPs (1 mg/mL) were exposed for 900 s and Milli-Q water was subtracted as buffer background and used for absolute scale calibration. Data analysis was performed with the program package SUPERSAXS developed in-house (Oliveira, C. L. P.; Pedersen, J. S., unpublished).

2.6. Cell culture

The murine macrophage cell line RAW 264.7 was purchased from the American Type Culture Collection (TIP71, Manassas, VA, USA). The cells were maintained in Dulbecco's Modified Eagle's Medium (DMEM, Fisher Scientific Biotech Line, Slangerup, Denmark) and supplemented with 100 U/mL penicillin, 100 µg/mL streptomycin, 2 mM glutamine (all from Sigma-Aldrich) and 10% (v/v) fetal bovine serum (FBS, PAA Laboratories, Pasching, Austria). The cells were grown in a 5% CO_2–95% atmospheric air incubator at 37 °C, the growth medium was renewed every second day, and the cells were sub-cultured twice a week by detaching them from the culture flask by scraping.

2.7. Determination of silencing efficiency in vitro

Silencing of TNF expression in activated RAW 264.7 cells was determined essentially as previously described [10,17]. In brief, cells were seeded in 24-well tissue culture plates (Sigma) at a density of 1.0×10^5 cells per well and incubated overnight. Subsequently, nanoparticle suspensions were added to each well in triplicates, resulting in a final siRNA concentration of 100 nM, and then the cells were incubated for 21 h. To each well, 5 ng/mL (final concentration) LPS (Sigma-Aldrich) was added, and the cells were incubated for additional 3 h. Untreated cells were incubated with PBS, negative control cells received LPS but not siRNA or particles, and cells dosed with LPS and TNF siRNA complexed with Trans-IT TKO (Mirus Corp, Madison, WI, USA) served as the positive control. In addition, cells transfected with NPs loaded with scrambled siRNA were used as negative control. RNA was isolated and purified using the RNA Stat-60 (AMS Biotechnology, Abingdon, UK), and reverse transcription of RNA was performed by applying the iScript cDNA synthesis kit (Bio-Rad Laboratories, Hercules, CA, USA). The PCR reactions were conducted in duplicates using a LightCycler® 480 (Roche, Basel, Switzerland) and the SYBR Green® Master mix (Roche). The reference genes β-actin (ACT) and β-glucuronidase (GUS) were used for normalization. The LightCycler® 480 software v.1.5.0 (Roche) was used for crossing point (*CP*) analysis, followed by quantification relative to the LPS-treated cells using the comparative $\Delta\Delta CP$ method as previously described [10,17]. The concentrations corresponding to 50% TNF silencing (IC_{50} values) for the dose-response curves were calculated using curve fitting algorithms (GraphPad Prism, La Jolla, CA, USA).

2.8. Viability assay

The effect of LPNs and SNALPs on the viability of RAW 264.7 cells was determined using the 3-(4,5-dimethylthiazol-2-yl)-2,5-diphenyltetrazolium bromide (MTT) assay. RAW 264.7 cells were seeded at a density of 10,000 cells per well in 96-well plates and cultured for 24 h. The cells were incubated with dispersions of LPNs or SNALPs in medium at different TNF siRNA concentrations for 24 h at 37 °C. Cells incubated with lipofectamine2000 (Invitrogen) were used as positive control, while untreated cells were used as negative control. After incubation, the cells were washed with PBS, and 100 µL of freshly prepared MTT reagent in HBSS buffer was added to each well followed by incubation at 37 °C for 4 h. The cell viability was determined by measuring the absorbance of the solubilized formazan at 595 nm.

2.9. Cell apoptosis and necrosis analysis

Cell apoptosis and necrosis were determined essentially as described previously [10,17]. RAW 264.7 cells were seeded in 24-well culture plates (Sigma) at a concentration of 4.0×10^5 cells per well. The apoptosis of cells, exposed to LPNs and SNALPs (at TNF siRNA concentrations of 100, 200, 400, and 800 nM) for 24 h, was determined. After treatment, cells were collected, washed with PBS, and stained with FITC-labeled Annexin V and propidium iodide (Life Technologies, Carlsbad, CA, USA) following the manufacturer's instructions. The numbers of cells undergoing necrosis (positive for propidium iodide), early apoptosis (positive for Annexin V), and late apoptosis (double-positive for Annexin V and propidium iodide) were quantified by flow cytometry using a Gallios flow cytometer (Beckman Coulter, Brea, CA, USA) as previously described [10,17].

2.10. Cell uptake

Cellular association of siRNA was quantified by using flow cytometry. RAW 264.7 cells were seeded in 24-well plates (2.0×10^5 cells per well) 24 h before the experiment, which was initiated by incubating the cells with nanoparticles at a concentration of 100 nM Alexa647-labelled siRNA in medium at 37 °C for 0.5, 1, 3, 6 and 24 h. Cells were rinsed twice with PBS, scraped and diluted with medium. After washing and centrifugation, the cell pellet was resuspended in 200 µL PBS and analyzed by flow cytometry using a Gallios flow cytometer (Beckman Coulter) as previously described [18]. Data were analyzed using FlowJo 7.6.5 (Three Star, Ashland, OR, USA).

In the uptake experiments conducted at 4 °C, RAW 264.7 cells were preincubated in medium at 4 °C for 10 min before NP suspensions were added, and the cells were incubated for 3 h either at 37 or 4 °C. For the endocytic inhibition assays, RAW 264.7 cells were washed with PBS, and fresh medium was added containing endocytosis inhibitors as previously described [19]. The cells were treated with NPs in the absence or presence of endocytosis inhibitors including nystatin (20 µg/mL, Sigma) chlorpromazine (5 µg/mL, Sigma), cytochalasin D (2 µg/mL, Sigma), amiloride (100 µg/mL, Sigma) and dynasore (26 µg/mL, Sigma). The compounds were added to the cell culture medium 0.5 h prior to addition of the LPN or SNALP suspensions. The concentration of Alexa647 siRNA in the cell culture medium was 100 nM in all the experiments. The fluorescence level in the cells was determined after 3 h.

2.11. Cellular siRNA distribution

Confocal laser scanning microscopy was used to visualize uptake of Alexa647 siRNA in RAW 264.7 cells [18]. Cells were seeded in 12-well tissue culture plates containing a cover slip at a density of

4.0×10^5 cells per well. The cell culture medium was aspirated and replaced with fresh culture medium. Cells were incubated with NPs at a concentration equivalent to 100 nM of Alexa647 siRNA for 3 h at 37 °C. After incubation, the cells were washed three times with PBS and incubated for additional 1 h with Lysotracker DND99 (200 nM, Molecular Probes) to stain late endosomes and lysosomes. After washing with PBS, the cells were fixed with fresh 3% (v/v) paraformaldehyde, and the cells were incubated with 4́, 6-diamidino-2-phenylindole (DAPI, 0.2 μg/mL, Invitrogen) for 5 min to stain the nuclei. After washing, the cover slips were placed on a slide using the Vectashield® mounting medium (Vector Laboratories, Peterborough, UK). The cells were imaged by confocal microscopy using a Zeiss LSM 710 confocal microscope (Carl Zeiss, Jena, Germany). The obtained images were processed using the Zeiss Zen black 2012 software.

2.12. Mice

Female Balb/cAnNCrl mice, 18–20 weeks old were purchased from Charles River laboratories (Sulzfeld, Germany). Animals were fed *ad libitum*, housed in groups of six mice per cage and kept under standard conditions of the animal facility. All experiments were approved by the Animal Experiment Committee of Utrecht University (AVD108002016467).

2.13. Induction of PGIA

Human proteoglycan (hPG) was isolated from human articular cartilage as previously described [20]. To induce arthritis, Balb/c mice were injected twice intraperitoneally with a mixture of 2 mg dimethyldioctadecylammonium (DDA) (Sigma Aldrich) and 250 μg hPG with a 21 day interval [21]. Subsequently, mice were randomized among the experimental groups, and arthritis scores (0–4 per ankle, maximum score per mouse is 16, but the humane end point is 12) were determined three times a week in a blinded fashion using a visual scoring system based on swelling and redness of paws as previously described [22]. Briefly, the arthritis score is the result of the redness and swelling of each individual paw with a maximum score of 4 per paw. A score of 1 reflects mild inflammation (redness, swelling) of a single toe. A score of 2 represents either inflammation at two toes, or swelling and redness of the paw itself. A score of 3 reflects a more severe inflammation of both toes and the paw, and a score of 4 represents the maximal score, where the entire foot and all four toes are severely inflamed with significant reduced range of motion. Usually, the arthritis development in the individual paws follow different kinetics, and hence the scores can fluctuate in this relapsing and remitting model. NP dispersions (10 μL/mouse) were administered twice by intra-articular injection in the left ankle joint with 29G insulin syringes (1 mL, BD Medical, Le Pont de Claix Cedex, France) at day 25 and 27. The positive control group received three times a week an intraperitoneal injection with 125 μg dexamethasone in 100 μL PBS [23].

2.14. hPG ELISA

Blood was sampled from the submandibular vein of the mice by a cheek puncture on day 27 and 46. Serum was separated by centrifuging the blood at 10,000 g for 10 min. The hPG specific antibodies in serum were measured by enzyme-linked immunosorbent assay (ELISA). The hPG-specific IgG1 and IgG2a Ab levels were compared with a standard of pooled sera from arthritic mice. Flat-bottom Costar assay 96-well plates (Corning, Kennebunk, ME, USA) were coated with hPG (5 μg/mL), and the free binding sites were blocked with 1% BSA (Sigma Aldrich, St Louis, MO, USA) in PBS (Lonza, Maastricht, The Netherlands). Sera were applied in increasing dilutions, and levels of both total hPG-IgG and hPG-IgG2a were determined using horse radish peroxidase conjugated goat anti-mouse IgG2a (Southern biotech, Birmingham, USA). For detection, 2,2′-azinobis [3-ethylbenzothiazoline-6-sulfonic acid]-diammonium salt (ABTS, Roche, Woerden, The Netherlands) was used. Optical density was measured at 405 nm with a microplate reader (Bio-rad, 550 model).

2.15. Statistics

Experiments were performed in triplicate, and data are presented as mean values ± SD. The difference of experimental data between two groups was assessed using the two-tailed Student's *t* test, and one-way analysis of variance (ANOVA) followed by a Tukey's post hoc test was used to analyze the mean difference among groups. The statistical significance level was set to $p < 0.05$.

3. Results and discussion

3.1. Preparation of LPNs

A double emulsion solvent evaporation method was applied to prepare non-loaded and TNF siRNA-loaded, L_5-modified LPNs, as previously reported [12,14]. The mean hydrodynamic diameter (*z*-average) of the resulting nanoparticles was approximately 210 nm and the polydispersity index (PDI) was approximately 0.11, inferring relatively narrow size distributions (Table 1). We used the previously reported ethanol destabilization method to prepare L_5-based SNALPs [11,12]. Dynamic light scattering (DLS) results indicated that the average size of the siRNA-loaded SNALPs (74 ± 8 nm) was significantly smaller ($p < 0.001$) than the size of the LPNs (Table 1). The size distribution of the SNALPs was relatively narrow (PDI = 0.09 ± 0.01). The LPNs had a positive zeta potential (12.5 ± 6.5 mV), while the SNALPs displayed an almost neutral zeta potential (-1.3 ± 4.4 mV). The siRNA encapsulation efficiencies of the LPNs and SNALPs were 93.3 ± 5.7% and 84.9 ± 1.5%, respectively, indicating high siRNA entrapment efficiency for both types of nanoparticles (Table 1). An important observation is that the encapsulation efficiency measured for the TNF siRNA (93%) is higher than the encapsulation efficiency that we previously reported for an siRNA targeting enhanced green fluorescent protein (EGFP), as the latter LPNs displayed an encapsulation efficiency in the range of 60–80% [12]. We speculate that the encapsulation efficiency is sequence-specific and may depend, among other factors, on the chemical modification pattern of the bases, which influences the hydrophobicity and hence the siRNA encapsulation during emulsification. The practical siRNA loading was

Table 1
Physicochemical properties of nanoparticles (NPs). Data represent mean values ± standard deviation (SD, n = 3).

Formulation	*z*-average (nm)	PDI	Zeta potential (mV)	Encapsulation efficiency (%)	siRNA loading (μg/mg NPs)
PLGA NPs	195.6 ± 1.9	0.08 ± 0.01	−17.6 ± 1.1	–	–
Non-loaded LPNs [a]	174.7 ± 2.2	0.09 ± 0.01	19.5 ± 1.4	–	–
LPNs [a,b]	210.2 ± 9.1	0.11 ± 0.01	12.5 ± 6.5	93.3 ± 5.7	9.1 ± 0.6
SNALPs [c]	73.6 ± 8.2	0.09 ± 0.01	−1.3 ± 4.4	84.9 ± 1.5	98.9 ± 1.9

[a] L_5:total solid content of 15% (w/w).
[b] L_5:siRNA ratio 15:1 (w/w).
[c] siRNA:total lipids weight ratio 1:7.5.

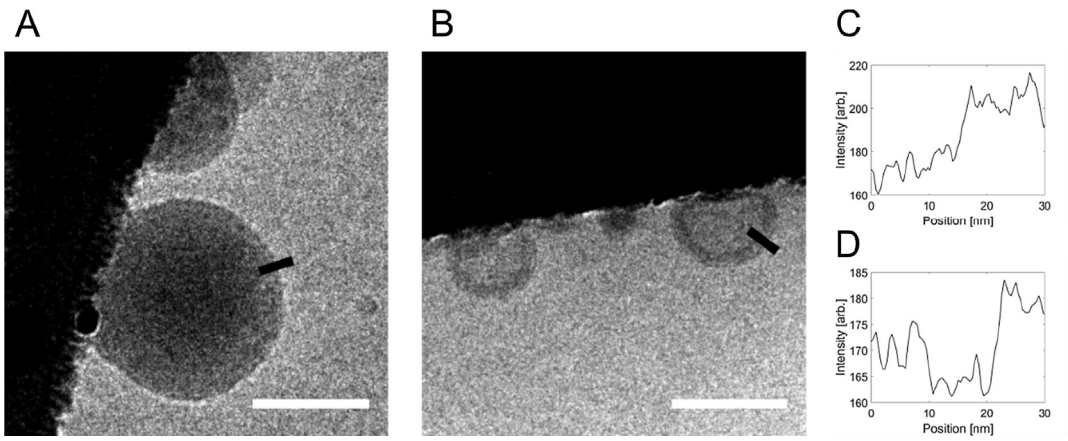

Fig. 1. Representative cryo-TEM images of siRNA-loaded LPNs (A) and SNALPs (B). Electron density profiles across the edge of particles (black lines) show a uniform structure of siRNA-loaded LPNs (C) and a core-shell structure of SNALPs (D). Scale bars = 100 nm.

approximately 10 times higher for the SNALPs than for the LPNs, as previously reported [12].

The shape, morphology and size of LPNs and SNALPs loaded with TNF siRNA were examined by cryo-TEM (Fig. 1). The LPNs were spherical (Fig. 1A), and the particle sizes corresponded to the size distributions and PDIs measured by dynamic light scattering (Table 1). We observed a pronounced structural difference between LPNs and SNALPs (Fig. 1A and B). The electron density profile across the surface of LPNs reveals a uniform structure (Fig. 1C), while the profile of SNALPs demonstrates that SNALPs are multilamellar vesicles with an outer shell of approximately 10 nm (Fig. 1D). No visual difference was evident between the appearance of the non-loaded LPNs and the corresponding nanocarriers loaded with siRNA cargo. A similar morphology was demonstrated in our recently reported cryo-TEM studies of lipidoid-modified LPNs [12]. Interestingly, previous SAXS studies indicated that lamellar lipid structures are present on the surface of DOTAP-modified LPNs [9]. The multilamellar vesicle model was proposed for the self-assembled SNALPs based on studies showing that the outer shell layer is composed of helper lipid and cationic lipid, while the nucleic acid cargo is localized between the onion-like lipid bilayers [24,25]. However, a nanostructure core model and a homogeneous core-shell model have also been proposed for such self-assembled lipid nanoparticles [26,27]. It must be noted that the preparation method, the specific type of lipids, the formulation parameters, and the specific RNA cargo significantly contribute to the cargo loading, the particle volume and the resulting particle structure.

3.2. Nanomechanical characterization of nanoparticle stiffness and adhesion

Characterization of the structure and stability of LPNs is essential for improving the understanding of the physicochemical and material properties of the LPNs, and they constitute important parameters for the ability of LPNs to efficiently deliver siRNA. The stiffness of nanoparticles may affect their cellular uptake. Soft particles tend to deform upon contact with the cellular membrane, which necessitates a higher energy required for cellular internalization, in comparison to rigid particles [28,29]. We examined the effect of L_5 and siRNA loading on the stiffness and adhesion of PLGA particles by using quantitative nanomechanical mapping (QNM), which is an atomic force microscopy (AFM)-based method [30]. The stiffness of the non-loaded PLGA particles was found to be 5.90 ± 1.44 GPa (mean value ± SD of the normal distribution, Fig. 2A and Table S2), corresponding to the stiffness reported for the bulk material [31]. Inclusion of L_5 in the particle structure resulted in a significantly decreased particle stiffness of 2.16 ± 0.57 GPa, which indicates that L_5 is either adsorbed to the PLGA surface or integrated in the particles. Subsequent loading of siRNA resulted in an increased stiffness of 3.48 ± 0.92 GPa. This is likely caused by a more dense packing of the cationic lipidoid due to reduction of electrostatic repulsion between cationic headgroups by the presence of anionic siRNA. This indicates that both L_5 and siRNA interact with the PLGA matrix of the LPNs. The opposite zeta potential of the LPNs with L_5 incorporated as compared to that of unmodified PLGA NPs (Table 1), shows that the cationic L_5 is located on the surface of the LPNs. However, the adhesion force measured between the silicon AFM probe and the PLGA NPs was not affected by the incorporation of L_5 and loading of siRNA (Table S2). This could indicate that the main parts of L_5 and siRNA are integrated within the bulk of the PLGA NPs, accounting for the lack of internal structure observed by cryo-TEM. SNALPs were deformed upon attachment to the surface used for the AFM studies. Therefore, the nanomechanical stiffness of SNALPs could not be accurately determined. In an AFM-based study of similar-sized vesicles composed of cationic DOTAP lipids, a stiffness of 20 MPa was reported [32], which is two orders of magnitude lower than the stiffness measured for LPNs in the present study. The deformation of SNALPs indicates a vesicle structure with a water core, as also inferred by the cryo-TEM studies. Hence, based on the composition and observed deformation, we consider SNALPs to be significantly softer than LPNs. Furthermore, compared to LPNs, a significantly stronger and more variable adhesion of SNALPs was observed (Fig. 2B and Table S2). The small negative zeta potential of SNALPs, combined with the variable adhesion, indicate that the surface presents both the cationic L_5 and anionic siRNA.

3.3. SAXS characterization of L_5 and siRNA loading in LPNs

To verify the formation of the bilayer structures observed by cryo-TEM and further investigate the packing of L_5 and siRNA, we characterized LPNs and SNALPs by SAXS. The SAXS data of the LPNs, displayed as intensity as a function of the modulus of the scattering vector, q, showed strong scattering at low -q values originating from the overall particle size in the nano range (Fig. 2C, cyan, red, and black curves). The smaller-sized SNALPs showed a distinctly different signal indicative of vesicular structures, where a low -q upturn, originating from the overall shape, was observed along with a characteristic broad bilayer core–shell cross-section bump in the medium q range (Fig. 2C, blue curve). No Bragg-like peaks were observed for the unmodified PLGA NPs (Fig. 2C, cyan curve), indicating that there is no ordered structural organization of the PLGA polymer on the nanometer length scale, in agreement with previously published results [8]. Inclusion of L_5 resulted in the appearance of peaks at q-values of approximately 0.0455 and 0.091 $Å^{-1}$, respectively (red curve). Using Bragg's law, these peaks can be assigned to structures with d spacings of approximately 138 Å and 69 Å, respectively (Fig. 2C, red curve, red arrows). Considering the

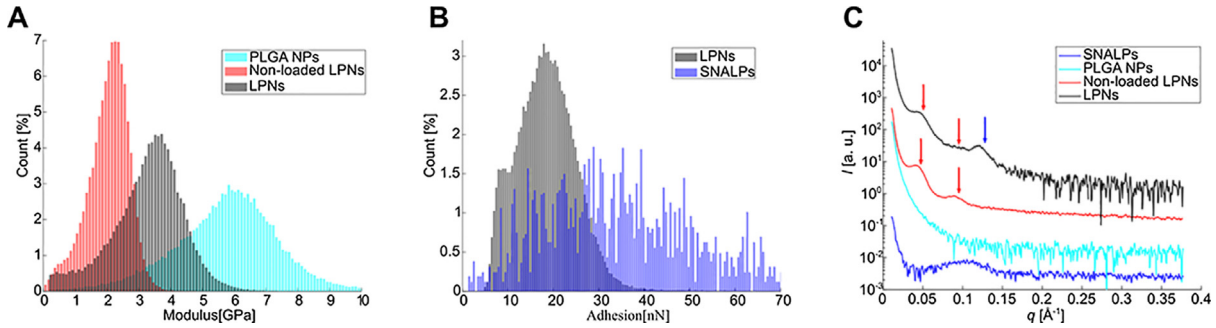

Fig. 2. (A) AFM-based nanomechanical stiffness characterization of unmodified PLGA NPs (cyan), non-loaded LPNs (red) and siRNA-loaded LPNs (black). (B) Adhesion of LPNs (black) and SNALPs (blue). (C) SAXS diffraction patterns for SNALPs (blue), PLGA NPs (cyan), non-loaded LPNs (red) and siRNA-loaded LPNs (black). Red and blue arrows, respectively, indicate the Bragg-like peaks corresponding to lamellar structures. (For interpretation of the references to color in this figure legend, the reader is referred to the web version of this article.)

amphiphilic structure of L_5, these peaks were identified as the characteristic first and second order reflection of a lamellar phase with a periodicity of approximately 69 Å. Lamellar L_5 structures have not previously been studied, but for dispersions of bulk L_5, we observed a periodic structure of approximately 50 Å (results not shown). Loading of siRNA into the LPNs resulted in the appearance of an additional broad peak at a *q*-value of 0.125 $Å^{-1}$, corresponding to a *d* spacing of 50 Å (blue arrow). The first and (less visible) second order peaks of L_5 were also present with *d* spacings of approximately 135 Å and 69 Å, respectively (Fig. 2C, black curve, red arrows). Therefore, these data suggest that L_5 forms a bilayer structure when included in the PLGA NPs. However, in the absence of counter charges, *e.g.*, provided by the siRNA, this structure has a significantly larger *d* spacing than the native bilayer, probably as a result of interbilayer repulsive electrostatic interactions between the cationic groups. Hence, the siRNA is integrated with the L_5 in the PLGA NPs, where bilayers of similar thickness as the native L_5 bilayers are formed. This is in agreement with our previous results, where it was observed that increased loading with siRNA resulted in a decreased thickness of the DOTAP bilayers in the LPNs [9]. The weak peak at a *d* spacing of approximately 69 Å could indicate the coexistence of non-complexed L_5. Further experiments are needed to elucidate the structural properties of L_5 in greater detail, as the molecule displays four amine functionalities and five hydrocarbon chains that could result in alternative structures in addition to the observed bilayer structure.

The SAXS data for the SNALPs (Fig. 2C, blue curve) were simplistically modeled using a single-layered polydisperse vesicle model to obtain information about the particle morphology and the bilayer cross-section structure. The fit suggested a vesicle diameter of approximately 76 nm, correlating well with the hydrodynamic diameter measured by DLS (Table 1), and a bilayer cross-section thickness of approximately 10 nm, which is in the same range as the width of the electron density distribution measured by using cryoTEM (Fig. 1B).

3.4. siRNA-loaded LPNs mediate dose-dependent TNF mRNA silencing

The ability of siRNA-loaded LPNs and SNALPs to mediate RNAi *in vitro* was evaluated in LPS-activated RAW 264.7 cells by real-time reverse transcription (RT) PCR as previously described [10,16]. The TNF silencing mediated by LPNs and SNALPs was dose-dependent (Fig. 3A). The half-maximal inhibitory concentration (IC_{50}) of LPNs (21.5 ± 2.2 nM) was significantly lower ($p < 0.05$) than the IC_{50} value of SNALPs (38.1 ± 5.3 nM). In comparison, we previously determined the TNF silencing mediated by DOTAP-modified LPNs using the same cell line and found an IC_{50} value > 100 nM [17]. Negative control LPNs loaded with scrambled siRNA did not induce any silencing of TNF expression, whereas the commercial siRNA transfection reagent TKO induced TNF silencing in a dose-dependent manner (Figure S1). These results indicate siRNA-dependent induction of RNAi mediated by LPNs and SNALPs. Our previous study showed that the IC_{50} value for the transfection efficiency of LPNs loaded with EGFP siRNA was in the range of 4–10 nM in the human non-small cell lung carcinoma cell line H1299 stably transfected with EGFP [12]. This discrepancy may be a result of cell line-dependent differences in transfection efficiency. The present study also shows that L_5-modified LPNs are much more efficient in mediating TNF silencing *in vitro* than DOTAP-modified LPNs, as also demonstrated for LPNs loaded with EGFP siRNA in H1299 cells stably transfected with EGFP [12].

Subsequently, the cell viability was examined in order to exclude that the observed TNF silencing effect was influenced by NP-induced toxicity. Cell viability measurements using the MTT assay showed that neither LPNs nor SNALPs caused any significant toxicity *in vitro* in RAW 264.7 cells in the tested concentration range (Fig. S2). Potential apoptotic and necrotic effects of the particles, which may not be apparent from the MTT assay, were investigated by flow cytometry using a combination of fluorescein isothiocyanate (FITC)-labeled annexin V and propidium iodide (Fig. S3). Compared with the negative control (PBS), no significant apoptosis or necrosis was observed for LPNs or SNALPs at siRNA concentrations of 100 nM and 200 nM, respectively (Fig. 3B). At the highest siRNA concentration tested (400 nM), both types of particles induced low levels of apoptosis (< 10%). In addition, a significant increase in induced apoptosis/necrosis was observed for SNALPs as compared to that found for LPNs at an siRNA concentration of up to 800 nM ($p < 0.01$). Induction of apoptosis or necrosis at such high concentrations could be attributed to the undesired side effects mediated by the cationic lipidoid component of the LPNs [13].

3.5. RAW 264.7 cells internalize siRNA more efficiently when encapsulated in LPNs and SNALPs, and the NP-mediated uptake is energy-dependent

To quantitatively investigate cellular uptake in RAW 264.7 cells, Alexa647-labelled siRNA was loaded in LPNs and SNALPs, respectively, and the uptake in cultured living cells was compared to the uptake of unloaded Alexa647-labelled siRNA by measuring the Alexa647 fluorescence intensity after incubation for 0.5, 1, 3, 6, and 24 h (Fig. 4A). After a relatively short incubation period (0.5 and 1 h), the levels of cellular siRNA delivered by LPNs appeared to be higher than the levels delivered by SNALPs. However, the cellular levels of siRNA were significantly higher in the case of SNALPs after continued treatment in new culture medium for 3, 6, or 24 h. The uptake data were analyzed using pseudo-first and pseudo-second order kinetics, which have been employed to characterize uptake profiles [33]. The LPNs and SNALPs tended to exhibit pseudo-first order uptake characteristics (Fig. 4A). In a pseudo-first order model, the fraction of intracellular siRNA delivered by LPNs and SNALPs increases exponentially as a function of incubation time, and the uptake efficiency is dependent on the specific type of NPs. In addition, the r^2 values of fits in both models for the unloaded siRNA were found to be < 0.9, indicating that the uptake of unloaded siRNA

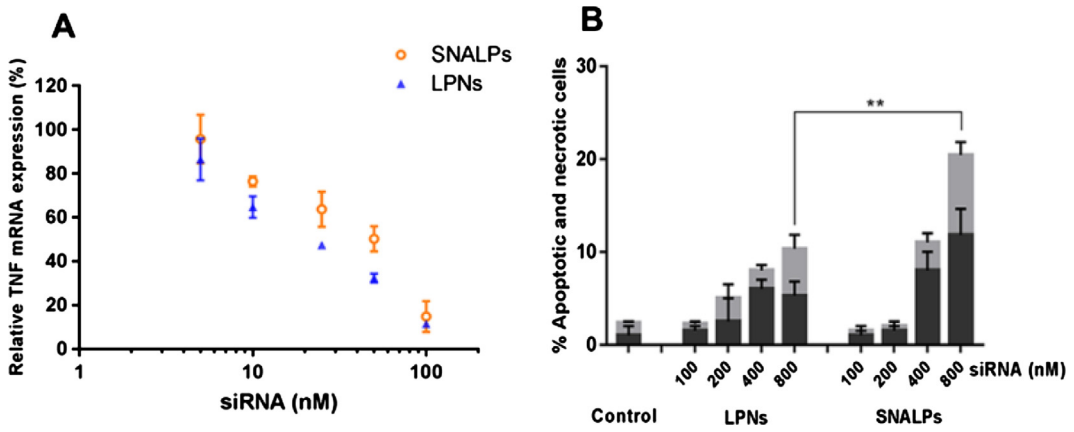

Fig. 3. (A) TNF mRNA silencing in RAW 264.7 cells incubated with LPNs (blue triangles) or SNALPs (orange circles). Results are normalized to non-transfected, LPS-treated cells (100%). (B) Comparison of apoptotic (black) and necrotic (grey) cells for RAW 264.7 cells incubated with LPNs and SNALPs for 24 h, respectively, measured relative (in percentage) to the values for untreated RAW 264.7 cells (control). Data represent mean values ± SD (n = 3). $^{**}p < 0.01$. (For interpretation of the references to color in this figure legend, the reader is referred to the web version of this article.)

neither follows pseudo-first order nor pseudo-second order kinetics. In contrast, very little unloaded siRNA was taken up by RAW 264.7 cells, which is consistent with the hypothesis that large biomolecules like siRNA are hardly endocytosed by cells [34]. To investigate the energy dependency of the cellular internalization, the uptake of the particles was compared at 4 and 37 °C. Endocytosis is an energy-dependent process that is inhibited at low temperatures [35]. There was a remarkable reduction of intracellular siRNA accumulation at 4 °C (which was 88% for LPNs and 98% for SNALPs, respectively) as compared to the experiments performed at 37 °C (Fig. 4B). These findings indicate that both LPNs and SNALPs are internalized via energy-dependent processes. SNALPs are softer than LPNs and deform significantly when imaged by AFM. It is possible that SNALPs will also deform upon contact with the cell membrane, which requires more

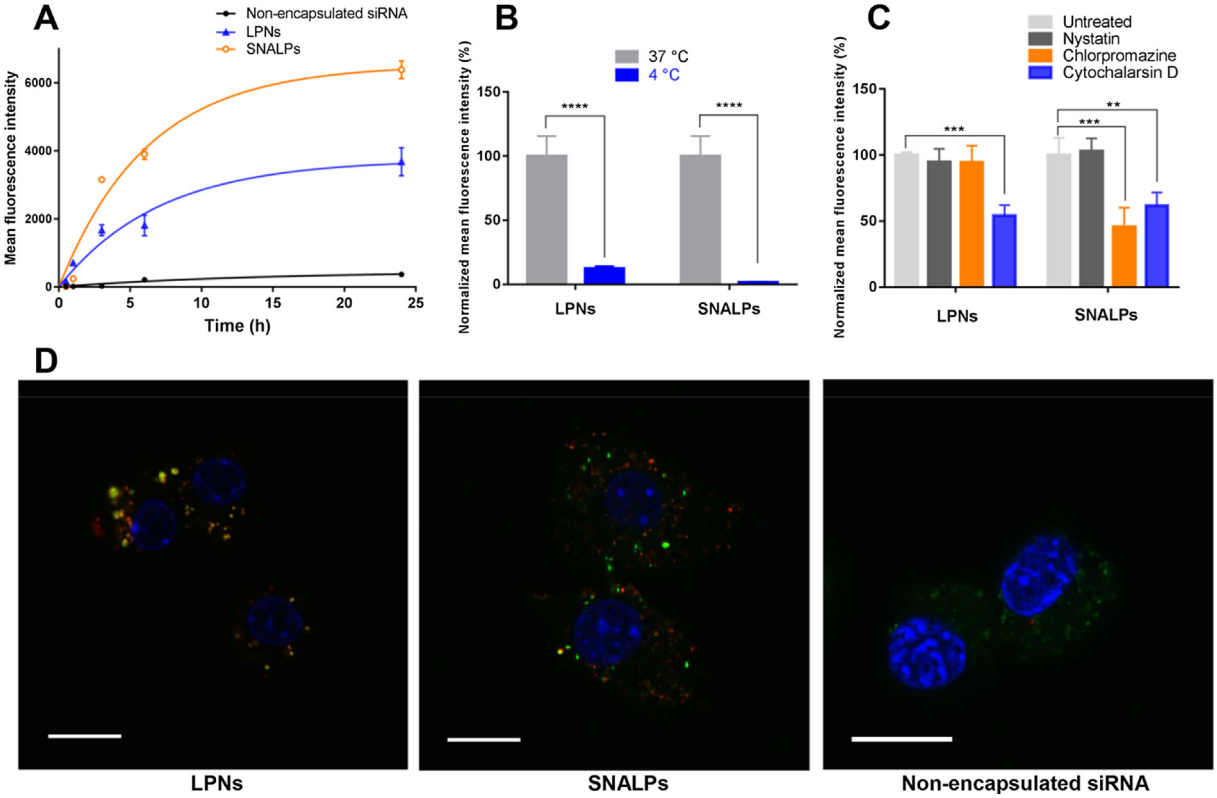

Fig. 4. (A) Intracellular Alexa647 siRNA level in RAW 264.7 cells exposed to non-encapsulated Alexa647 siRNA, LPNs and SNALPs, respectively for 0.5, 1, 3, 6, and 24 h at 37 °C, and plot of the data with nonlinear regression fits (full lines). (B) Endocytosis of NPs loaded with Alexa647 siRNA at 4 °C. Cells were pretreated at 4 °C for 10 min prior to subsequent incubation of NPs at 4 °C for 3 h. $^{****}p < 0.0001$ when compared with cells incubated at 37 °C. (C) RAW 264.7 cells were pre-incubated with inhibitors for 0.5 h, and they were subsequently cultured in medium containing NPs. The concentration of Alexa647 siRNA in the cell culture medium was 100 nM in all the experiments. The fluorescence level of Alexa647 siRNA was determined at 3 h. $^{**}p < 0.01$, $^{***}p < 0.001$, as compared to untreated cells. Data represent mean ± SD (n = 3). D) Representative confocal microscopy images of RAW 264.7 cells (blue: nuclei) transfected with LPNs, SNALPs and non-encapsulated Alexa647 siRNA, respectively. In all experiments a concentration of 100 nM Alexa647 siRNA was used. The co-localization patterns (yellow) of siRNA (red) with LysoTracker (late endosome/lysosome marker, green) 3 h after treatment with NPs show different intracellular siRNA distribution patterns. Scale bars = 20 μm. (For interpretation of the references to color in this figure legend, the reader is referred to the web version of this article.)

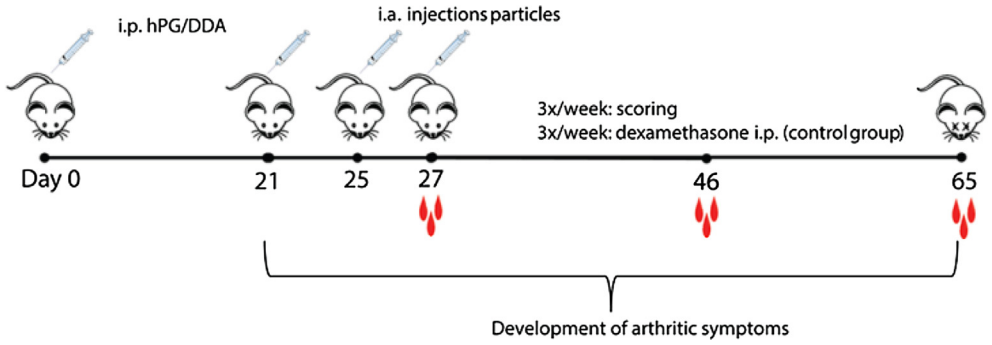

Fig. 5. Experimental scheme. Mice were immunized twice intraperitoneally (i.p.) with a mixture of 250 μg hPG and 2 mg DDA at day 0 and day 21. The mice were dosed twice at day 25 and day 27 with the different treatments. From day 21, the animals were scored three times a week for arthritis symptoms. As positive control, animals were dosed i.p. three times a week with 125 μg dexamethasone from day 21. Blood samples were collected at day 27 and 46 for measurement of hPG-specific antibodies. Animals were euthanized at day 65, and hPG-specific antibodies were measured in the blood.

energy for cellular internalization, as compared to uptake of LPNs. This matches the higher reduction in the uptake of SNALPs, as compared to that of LPNs, at low temperature. However, further studies are needed to systematically investigate the influence of particle stiffness on the cellular uptake.

3.6. Macropinocytosis and clathrin-mediated endocytosis are possible mechanisms involved in the uptake of LPNs and SNALPs

A considerable difference between the siRNA uptake profiles of the LPNs and SNALPs was noted, indicating that the siRNA delivery mediated by these two types of nanoparticles is likely to involve different endocytic pathways. Hence, we performed selective inhibition assays to elucidate which endocytic pathways are involved in the cellular internalization of lipidoid-based nanoparticles [19]. We studied the effects of selective inhibitors of macropinosome-mediated endocytosis (*i.e.*, cytochalasin D), clathrin-mediated endocytosis (*i.e.*, chlorpromazine), or caveolae-mediated endocytosis (*i.e.*, nystatin) on the uptake of Alexa647-labeled siRNA-loaded LPNs and SNALPs in RAW 264.7 cells (Fig. 4C). In comparison to cell-associated fluorescence in the absence of inhibitors, treatment with cytochalasin D led to reduced siRNA uptake, suggesting that the cellular uptake pathway for LPNs and SNALPs may be macropinocytosis (Fig. 4C). Furthermore, a significant decrease in SNALP-associated fluorescence was observed for cells treated with chlorpromazine (Fig. 4C). Therefore, clathrin-mediated endocytosis may also contribute to the uptake of SNALPs in RAW 264.7 cells. In contrast, incubation with nystatin did not influence cellular internalization, which infers that caveolae-mediated endocytosis is not involved in uptake. The effects of amiloride (an inhibitor of macropinosome-mediated endocytosis) and dynasore (an inhibitor of clathrin-mediated endocytosis) treatment on the uptake of nanoparticles in RAW 264.7 cells were also studied. The obtained results demonstrated comparable endocytic pathways for LPNs and SNALPs (Fig. S4). The experimental results indicate that macropinocytosis appears to be the primary endocytic mechanism for uptake of both LPNs and SNALPs in RAW 264.7 cells. This is probably a result of the unique phagocytic capacity of macrophages, which generally serve as scavengers by engulfing foreign particles [35]. In addition, the particle size is a major parameter affecting endocytosis of NPs [36]. Clathrin-coated vesicles have a general diameter of approximately 150 nm [36]. Since the diameter of SNALPs is in the range of 60–80 nm, it is likely that clathrin-coated vesicles may also be involved in the intracellular trafficking of SNALPs. Likewise, lipid NPs with an average diameter of approximately 60 nm have been shown to enter cells via clathrin-mediated endocytosis, as well as macropinocytosis [37]. Apart from inhibitors, endocytic markers and endogenous protein knock-out cell lines may also be employed to verify or exclude specific endocytic pathways for nanomedicines [38]. The mechanisms of LPN uptake in cell culture remain to a large extent unknown, and further studies are needed to elucidate the exact endocytosis mechanisms. The present results suggest that SNALPs mediate significant higher cellular uptake of siRNA than LPNs. However, the transfection efficiency of SNALPs (IC_{50} of 38.1 ± 5.3 nM) is much lower than that of LPNs (IC_{50} of 21.5 ± 2.2 nM), which may be attributed to a higher intracellular delivery capacity of LPNs.

To examine further how LPNs and SNALPs are taken up by antigen-presenting cells, we used confocal microscopy to investigate qualitatively their distribution and extent of cellular accumulation in RAW 264.7 cells upon incubation for 3 h at concentrations corresponding to 100 nM Alexa647 siRNA (Fig. 4D). A strong red fluorescence signal from Alexa647 siRNA was observed in RAW 264.7 cells incubated with both types of nanoparticles (Fig. 4D), indicating that both LPNs and SNALPs mediate intracellular delivery of a considerable amount of siRNA. In contrast, only a weak fluorescence signal was present in cells treated with non-encapsulated siRNA, which confirms that the use of a delivery system is important for siRNA transfection. In order to obtain more details on the intracellular trafficking of the particles, we performed co-localization studies using lysotracker to distinguish labeled siRNA present in endosomes and lysosomes. Co-localization of the fluorescence signals (yellow color) from Alexa647 siRNA and lysotracker demonstrates that both LPNs and SNALPs may be transported to late endosomes and lysosomes following endocytosis in RAW 264.7 cells (Fig. 4D). In addition, red fluorescence signals from Alexa647 siRNA were observed in cells treated with LPNs and SNALPs, which indicates that siRNA escapes from the lysosomes into the cytosol.

3.7. LPNs and SNALPs loaded with TNF siRNA reduce experimental arthritis in vivo after intra-articular administration

To test the effect of TNF siRNA-loaded LPNs and SNALPs on arthritis progression, we made use of the proteoglycan-induced arthritis (PGIA) model [21]. Arthritis was induced by intraperitoneal injection (i.p.) of a mixture of hPG and DDA. After two injections with hPG/DDA (on day 0 and day 21), the mice were dosed twice (on day 25 and day 27) with LPNs or SNALPs loaded with TNF siRNA or scrambled siRNA, while non-encapsulated siRNA was used as control (Fig. 5). Local administration was performed via intra-articular injections, where dose volumes of 10 μL of the nanoparticle dispersions or non-encapsulated siRNA were injected, respectively. As positive control, mice were injected three times a week until termination of the experiment (day 65) with dexamethasone, which is an immune-suppressing drug used for RA treatment. This dexamethasone dosing regimen has previously been shown to result in complete immune-suppression [23] Dexamethasone has a relatively short plasma half-life; hence, frequent administration is required for optimal efficacy. The treatment with dexamethasone was initiated four days earlier than the other treatments to obtain maximal immunosuppressive activity and to prevent induction of autoimmunity. Hence, this dosing regimen induces the maximal suppression of disease. From day 23 onwards, mice were scored three times a week for arthritic symptoms to monitor disease progression.

Mice that were dosed twice with LPNs or SNALPs (loaded with 1 μg TNF siRNA) showed significantly less arthritic symptoms than the

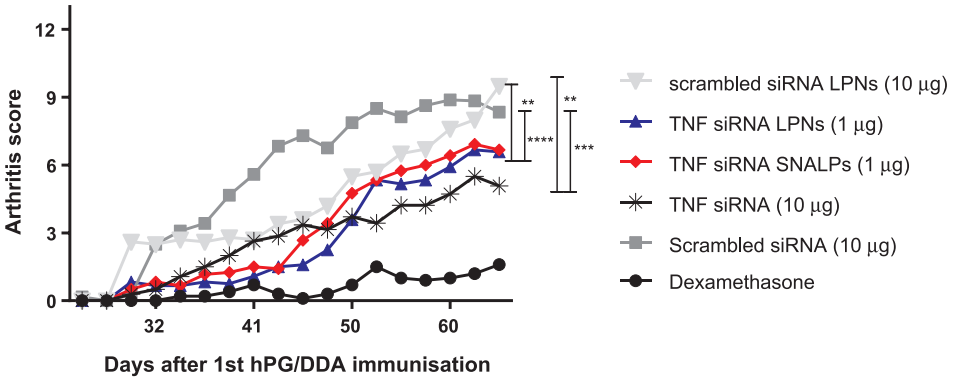

Fig. 6. Therapeutic effect of TNF siRNA-loaded LPNs and SNALPs *in vivo*, shown as the arthritis score as a function of the number of days after the first hPG/DDA immunization. Two intra-articular injections were given in the left ankle joint of the mice at day 25 and 27 of LPNs (1 µg siRNA, blue triangles), SNALPs (1 µg siRNA, red diamonds) and non-encapsulated TNF siRNA (10 µg siRNA, black asterisks); this reduced arthritis compared to the control groups treated with scrambled siRNA (10 µg siRNA, grey squares) and LPNs loaded with scrambled siRNA (10 µg siRNA, grey inverted triangles). As positive control, animals were treated three times a week with dexamethasone by intraperitoneal injection (125 µg in 100 µL PBS, black circles). The control groups are shown in all plots. Statistical analysis at day 65: two-way analysis of variance (ANOVA) and Tukey's post hoc test. Data represent mean values, n = 6. $^{**}p < 0.01$, and $^{****}p < 0.0001$. (For interpretation of the references to color in this figure legend, the reader is referred to the web version of this article.)

control groups (Fig. 6). In contrast, mice that were dosed twice with TNF siRNA loaded in DOTAP-modified PLGA NPs did not show reduced arthritis (Fig. S4). The explanation for this is that the DOTAP-modified LPNs are not as efficient in mediating gene silencing as the L_5-modified LPNs, as shown by us previously [12], and as demonstrated clearly in the present work. Therefore, higher doses of siRNA are needed for the formulation based on DOTAP-modified LPNs to achieve *in vivo* efficacy [10]. Although non-encapsulated TNF siRNA alone also reduced arthritic symptoms (Fig. 6), it should be noted that the dose of the non-encapsulated TNF siRNA was ten times higher than the siRNA dose of the administered NP dispersions (10 µg vs 1 µg). For the treated paws only, the same effects were observed (Fig. S6), although the differences were less pronounced due to the inherent problem related to intraarticular injection, which also induces swelling of the joints in some cases, eventually hampering the clinical scoring and reducing the apparent treatment efficacy. These results show that L_5-modified LPNs loaded with siRNA deliver their cargo efficiently *in vivo,* and that two locally administered doses are sufficient for therapeutic efficacy, which is attractive from a clinical perspective. The effect of repeated dosing (> 2 doses) could not be tested in the present studies, because only two injections were allowed for ethical reasons.

Furthermore, mice that were treated with TNF siRNA encapsulated in SNALPs or LPNs did not only show a reduced disease severity (as shown by the maximum arthritis score) but also a delayed onset of arthritis (Table 2). Mice that were injected with non-encapsulated TNF siRNA experienced the first arthritic symptoms at a similar time point as the control groups treated with scrambled non-encapsulated siRNA. This indicates that loading of siRNA in NPs enhances the delivery of the siRNA also *in vivo*. In contrast, mice that received a higher dose of NPs, corresponding to 10 µg siRNA, showed inflammatory symptoms immediately after injection (data not shown), indicating that this dose induces immune activation. Since the results showed a systemic effect of the NPs (when the arthritis score from the injected paw was subtracted, the mice that received LPNs and SNALPs containing TNF siRNA remained significantly less sick than the control groups), systemic administration of the cargo would be an option in future experiments [39]. Additional studies are needed for pharmacokinetic profiling of the siRNA and the nanoparticles after intraarticular injection.

Table 2
Maximum arthritis score and day of onset of disease. Data represent mean values ± SD (n = 6). As day of onset of disease is considered the first day on which a mouse has a score of 1 or more at one of the paws or toes. The maximum arthritis score is the maximum arthritis score during the entire experiment (i.e., not at the day of euthanization).

Treatment	Maximum arthritis score	Day of onset
Dexamethasone	1.7 ± 0.9	50.0 ± 6.6
TNF siRNA SNALPs (1 µg)	7.4 ± 3.2	43.2 ± 7.8
TNF siRNA LPNs (1 µg)	7.4 ± 2.7	46.3 ± 9.4
TNF siRNA (10 µg)	6.1 ± 3.9	35.3 ± 5.4
Scrambled siRNA LPNs (10 µg)	10.0 ± 2.4	33.0 ± 8.0
Scrambled siRNA (10 µg)	10.9 ± 1.6	35.3 ± 4.9

3.8. Snalps reduce the Th1-mediated immune response

Besides the disease-suppressing effects, it was tested whether TNF siRNA loaded in LPNs and SNALPs, respectively, could modify the adaptive immune response. To determine whether TNF siRNA treatment had an effect on antibody production, we compared serum antibody levels at three different time points (t = 27, 46, and 65 days, respectively, Fig. 7). Disease-inducing, hPG-specific IgG2a antibodies were measured for all groups and time points. At the first time points (t = 27 and 46 days), there were no significant differences in the levels of hPG-specific IgG2a antibodies between the groups. However, at the last time point (t = 65 days), the mice that were dosed with TNF siRNA loaded in SNALPs showed a significantly decreased level of hPG-specific IgG2a antibodies similar to the positive control group treated with dexamethasone. Treatment with non-encapsulated TNF siRNA or LPNs loaded with TNF siRNA did not reduce the hPG-specific IgG2a antibody levels in serum, as compared to the antibody levels measured for the control group treated with scrambled, non-encapsulated siRNA. In the applied PGIA model, mice that accommodate a response against autologous proteoglycan, and thus develop arthritic symptoms, have been shown to exhibit an increase in Th1-supported IgG2a antibodies [40]. As shown by the measurements in serum, SNALPs but not LPNs influence the production of hPG-specific-IgG2a antibodies (Fig. 7). Since IgG2a antibodies are driven by the Th1 cytokine interferon γ (IFN-γ), it is possible that SNALPs inhibit the production or neutralize this cytokine, whereas non-encapsulated TNF siRNA and LPNs containing TNF siRNA do not affect IFN-γ [41]. Therefore, the effects evident from the *in vivo* scoring cannot solely be attributed to a Th1-inhibiting effect. Furthermore, no differences in the levels of hPG-specific IgG1 antibodies were observed (data not shown), which indicates that non-encapsulated TNF siRNA, TNF siRNA-loaded LPNs, and TNF siRNA-loaded SNALPs do not affect the Th2 response. Further *in vivo* experiments are required to address in more details the T-cell differentiation after treatment, and to study both the inhibition of pro-inflammatory effector T cells and possible induction of regulatory T cells in the PGIA model.

4. Conclusions

In conclusion, we have designed a new type of lipidoid-based LPNs, for which the siRNA delivery efficiency was compared to that of SNALP nanoparticles. LPNs were larger in size and more stable than SNALPs, and siRNA was incorporated into the particle matrix as opposed to being displayed mainly on the surface of SNALPs, as seen from cryo-

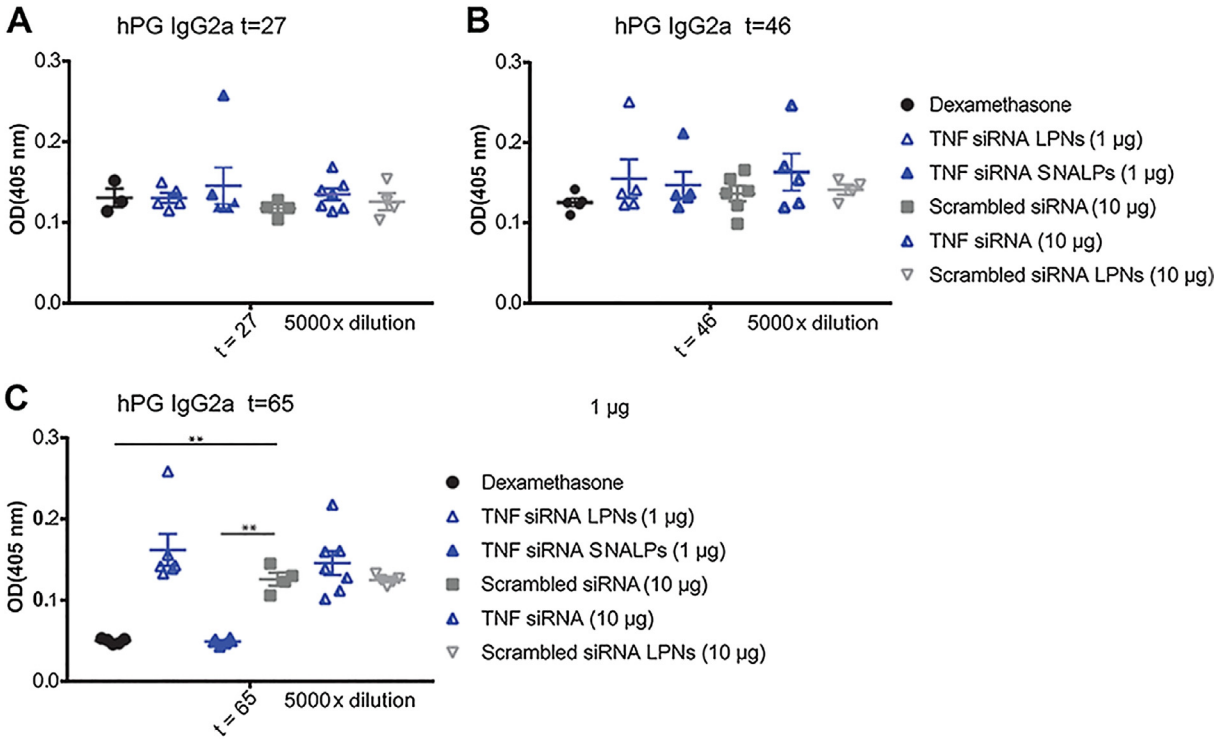

Fig. 7. Treatment with SNALPs loaded with TNF siRNA reduces the levels of hPG-specific IgG2a antibodies. hPG-specific IgG2a antibodies were measured in serum at day 27, 46, and 65. At the first two time points (A and B), there was no statistically significant differences in the hPG IgG2a antibody levels between the groups. However, on day 65 (C), the mice treated with TNF siRNA encapsulated in SNALPs (filled upward triangles) showed antibody levels comparable to the positive control group (dexamethasone, filled circles), which were significantly lower than the levels measured for the group treated with scrambled non-encapsulated siRNA (filled squares). Optical density (OD) was measured at 405 nm. Statistical analysis: two-way analysis of variance (ANOVA) and Tukey's post hoc test. Bars represent mean values ± SD, n = 6. $^{**}p < 0.01$.

TEM and validated by AFM and SAXS experiments. The *in vitro* experiments show that both LPNs and SNALPs are efficient delivery systems for TNF siRNA due to their ability to reduce the expression of TNF in LPS-activated macrophages. Both particle types were taken up via macropinocytosis, while only SNALPs could be taken up via clathrin-mediated endocytosis. *In vivo* results indicate that two doses of LPNs and SNALPs administered locally by intraarticular injection can efficiently suppress inflammation in an experimental arthritis model at a relatively low TNF siRNA dose (1 µg). Furthermore, treatment with SNALPs lead to a reduced Th1 response. However, additional studies are required to optimize the dosage regimen towards efficacious and safe treatment. These findings may guide future rational design of lipidoid-based nanocarriers for siRNA delivery in chronic inflammatory disorders and autoimmune diseases.

Declaration of interest

All authors report no potential conflicts.

Acknowledgements

We gratefully acknowledge the support from the Danish Council for Independent Research and FP7 Marie Curie Actions – COFUND (grant number DFF-4093-00292), the Lundbeck Foundation - Denmark (grant numbers R181-2014-3793 and R219-2016-908), Hørslev-Fonden – Denmark, the Carlsberg Foundation – Denmark, and the Novo Nordisk Foundation – Denmark (grant number NNF17OC0026526). We are also thankful to the Innovative Medicines Initiative Joint Undertaking under grant agreement no. 115363 resources which are composed of the financial contribution from the European Union's Seventh Framework Programme (FP7/2007-2013) and EFPIA companies' in kind contributions. LHK acknowledges support from the Carlsberg Foundation Internationalization fellowships (CF16-0757). This project has received funding from the European Union's Seventh Framework Programme for research, technological development and demonstration under grant agreement no. 600207. We acknowledge the Core Facility for Integrated Microscopy, Faculty of Health and Medical Sciences, University of Copenhagen and the skilled technical assistance of Klaus Qvortrup. We are grateful to Emily Falkenberg for synthesizing and purifying L5. Furthermore, we thank Dr Irene Ludwig for technical assistance during the in vivo experiments and the Dutch Arthritis foundation for financial support.

Appendix A. Supplementary material

Supplementary data to this article can be found online at https://doi.org/10.1016/j.ejpb.2019.06.009.

References

[1] D. Aletaha, T. Neogi, A.J. Silman, J. Funovits, D.T. Felson, C.O. Bingham III, N.S. Birnbaum, G.R. Burmester, V.P. Bykerk, M.D. Cohen, B. Combe, K.H. Costenbader, M. Dougados, P. Emery, G. Ferraccioli, J.M. Hazes, K. Hobbs, T.W. Huizinga, A. Kavanaugh, J. Kay, T.K. Kvien, T. Laing, P. Mease, H.A. Menard, L.W. Moreland, R.L. Naden, T. Pincus, J.S. Smolen, E. Stanislawska-Biernat, D. Symmons, P.P. Tak, K.S. Upchurch, J. Vencovsky, F. Wolfe, G. Hawker, rheumatoid arthritis classification criteria: an American college of rheumatology/European league against rheumatism collaborative initiative, Ann. Rheum. Dis. 69 (2010) (2010) 1580–1588.

[2] C. Tetta, G. Camussi, V. Modena, V.C. Di, C. Baglioni, Tumour necrosis factor in serum and synovial fluid of patients with active and severe rheumatoid arthritis, Ann. Rheum. Dis. 49 (1990) 665–667.

[3] S.M. van der Kooij, C.S. Le, Y.P. Goekoop-Ruiterman, J.K. de Vries-Bouwstra, Z.D. Van, P.J. Kerstens, J.M. Hazes, S.D. Van, F.C. Breedveld, B.A. Dijkmans, C.F. Allaart, Clinical and radiological efficacy of initial vs delayed treatment with infliximab plus methotrexate in patients with early rheumatoid arthritis, Ann. Rheum. Dis. 68 (2009) 1153–1158.

[4] M.E. Weinblatt, J.M. Bathon, J.M. Kremer, R.M. Fleischmann, M.H. Schiff,

R.W. Martin, S.W. Baumgartner, G.S. Park, E.L. Mancini, M.C. Genovese, Safety and efficacy of etanercept beyond 10 years of therapy in North American patients with early and longstanding rheumatoid arthritis, Arthritis Care Res. 63 (2011) 373–382.
[5] G.J. Wolbink, M. Vis, W. Lems, A.E. Voskuyl, G.E. De, M.T. Nurmohamed, S. Stapel, P.P. Tak, L. Aarden, B. Dijkmans, Development of antiinfliximab antibodies and relationship to clinical response in patients with rheumatoid arthritis, Arthritis Rheum. 54 (2006) 711–715.
[6] J. Sparks, G. Slobodkin, M. Matar, R. Congo, D. Ulkoski, A. Rea-Ramsey, C. Pence, J. Rice, D. McClure, K.J. Polach, E. Brunhoeber, L. Wilkinson, K. Wallace, K. Anwer, J.G. Fewell, Versatile cationic lipids for siRNA delivery, J. Control. Release 158 (2012) 269–276.
[7] K. Buyens, S.C. De Smedt, K. Braeckmans, J. Demeester, L. Peeters, L.A. van Grunsven, d.J. de Mollerat, X.R. Sawant, V. Torchilin, K. Farkasova, M. Ogris, N.N. Sanders, Liposome based systems for systemic siRNA delivery: stability in blood sets the requirements for optimal carrier design, J. Control. Release 158 (2012) 362–370.
[8] K. Bruno, Using drug-excipient interactions for siRNA delivery, Adv. Drug Deliv. Rev. 63 (2011) 1210–1226.
[9] S. Colombo, D. Cun, K. Remaut, M. Bunker, J. Zhang, B. Martin-Bertelsen, A. Yaghmur, K. Braeckmans, H.M. Nielsen, C. Foged, Mechanistic profiling of the siRNA delivery dynamics of lipid-polymer hybrid nanoparticles, J. Control. Release 201 (2015) 22–31.
[10] B.C. te Boekhorst, L.B. Jensen, S. Colombo, A.K. Varkouhi, R.M. Schiffelers, T. Lammers, G. Storm, H.M. Nielsen, G.J. Strijkers, C. Foged, K. Nicolay, MRI-assessed therapeutic effects of locally administered PLGA nanoparticles loaded with anti-inflammatory siRNA in a murine arthritis model, J. Control. Release 161 (2012) 772–780.
[11] A. Akinc, A. Zumbuehl, M. Goldberg, E.S. Leshchiner, V. Busini, N. Hossain, S.A. Bacallado, D.N. Nguyen, J. Fuller, R. Alvarez, A. Borodovsky, T. Borland, R. Constien, F.A. De, J.R. Dorkin, J.K. Narayanannair, M. Jayaraman, M. John, V. Koteliansky, M. Manoharan, L. Nechev, J. Qin, T. Racie, D. Raitcheva, K.G. Rajeev, D.W. Sah, J. Soutschek, I. Toudjarska, H.P. Vornlocher, T.S. Zimmermann, R. Langer, D.G. Anderson, A combinatorial library of lipid-like materials for delivery of RNAi therapeutics, Nat. Biotechnol. 26 (2008) 561–569.
[12] K. Thanki, X. Zeng, S. Justesen, S. Tejlmann, E. Falkenberg, E. Van Driessche, H.M. Nielsen, H. Franzyk, C. Foged, Engineering of small interfering RNA-loaded lipidoid-poly(DL-lactic-co-glycolic acid) hybrid nanoparticles for highly efficient and safe gene silencing: A quality by design-based approach, Eur. J. Pharm. Biopharm. 120 (2017) 22–33.
[13] A.M. de Groot, K. Thanki, M. Gangloff, E. Falkenberg, X. Zeng, D.C.J. van Bijnen, W. van Eden, H. Franzyk, H.M. Nielsen, F. Broere, N.J. Gay, C. Foged, A.J.A.M. Sijts, Immunogenicity testing of lipidoids in vitro and in silico: modulating lipidoid-mediated TLR4 activation by nanoparticle design, Mol. Ther. Nucleic Acids 11 (2018) 159–169.
[14] K. Thanki, X. Zeng, C. Foged, Preparation, characterization, and in vitro evaluation of lipidoid-polymer hybrid nanoparticles for siRNA delivery to the cytosol, Methods Mol. Biol. 2019 (1943) 141–152.
[15] J. Adamcik, A. Berquand, R. Mezzenga, Single-step direct measurement of amyloid fibrils stiffness by peak force quantitative nanomechanical atomic force microscopy, Appl. Phys. Lett. 98 (2011) 193701.
[16] J.S. Pedersen, A flux- and background-optimized version of the NanoSTAR small-angle X-ray scattering camera for solution scattering, J. Appl. Crystallogr. 98 (2004) 369–380.
[17] L.B. Jensen, J. Griger, B. Naeye, A.K. Varkouhi, K. Raemdonck, R. Schiffelers, T. Lammers, G. Storm, S.C. De Smedt, B.S. Sproat, H.M. Nielsen, C. Foged, Comparison of polymeric siRNA nanocarriers in a murine LPS-activated macrophage cell line: gene silencing, toxicity and off-target gene expression, Pharm. Res. 29 (2012) 669–682.
[18] X. Zeng, A.M. de Groot, A.J. Sijts, F. Broere, B.E. Oude, S. Colombo, E.W. Van, H. Franzyk, H.M. Nielsen, C. Foged, Surface coating of siRNA-peptidomimetic nano-self-assemblies with anionic lipid bilayers: enhanced gene silencing and reduced adverse effects in vitro, Nanoscale 7 (2015) 19687–19698.
[19] X. Zeng, Y. Zhang, A.M. Nystrom, Endocytic uptake and intracellular trafficking of bis-MPA-based hyperbranched copolymer micelles in breast cancer cells, Biomacromolecules 13 (2012) 3814–3822.
[20] A. Hanyecz, S.E. Berlo, S. Szanto, C.P. Broeren, K. Mikecz, T.T. Glant, Achievement of a synergistic adjuvant effect on arthritis induction by activation of innate immunity and forcing the immune response toward the Th1 phenotype, Arthrit. Rheum. 50 (2004) 1665–1676.
[21] M.J. van Herwijnen, L. Wieten, R. van der Zee, P.J. van Kooten, J.P. Wagenaar-Hilbers, A. Hoek, I. den Braber, S.M. Anderton, M. Singh, H.D. Meiring, C.A. van Els, W. van Eden, F. Broere, Regulatory T cells that recognize a ubiquitous stress-inducible self-antigen are long-lived suppressors of autoimmune arthritis, Proc. Natl. Acad. Sci. USA 109 (2012) 14134–14139.
[22] T.T. Glant, K. Mikecz, A. Arzoumanian, A.R. Poole, Proteoglycan-induced arthritis in BALB/c mice Clinical features and histopathology, Arthrit. Rheum. 30 (1987) 201–212.
[23] M. Koenen, S. Culemann, S. Vettorazzi, G. Caratti, L. Frappart, W. Baum, G. Kronke, U. Baschant, J.P. Tuckermann, Glucocorticoid receptor in stromal cells is essential for glucocorticoid-mediated suppression of inflammation in arthritis, Ann. Rheum. Dis. 77 (2018) 1610–1618.
[24] N. Maurer, K.F. Wong, H. Stark, L. Louie, D. McIntosh, T. Wong, P. Scherrer, S.C. Semple, P.R. Cullis, Spontaneous entrapment of polynucleotides upon electrostatic interaction with ethanol-destabilized cationic liposomes, Biophys. J. 80 (2001) 2310–2326.
[25] R. Crawford, B. Dogdas, E. Keough, R.M. Haas, W. Wepukhulu, S. Krotzer, P.A. Burke, L. Sepp-Lorenzino, A. Bagchi, B.J. Howell, Analysis of lipid nanoparticles by Cryo-EM for characterizing siRNA delivery vehicles, Int. J. Pharm. 403 (2011) 237–244.
[26] J. Viger-Gravel, A. Schantz, A.C. Pinon, A.J. Rossini, S. Schantz, L. Emsley, Structure of lipid nanoparticles containing siRNA or mRNA by dynamic nuclear polarization-enhanced NMR spectroscopy, J. Phys. Chem. B 122 (2018) 2073–2081.
[27] A.M. Yanez, T. Kjellman, S. Bartesaghi, S. Wallin, X. Wu, A.J. Kvist, A. Dabkowska, N. Szekely, A. Radulescu, J. Bergenholtz, L. Lindfors, Successful reprogramming of cellular protein production through mRNA delivered by functionalized lipid nanoparticles, Proc. Natl. Acad. Sci. USA 115 (2018) E3351–E3360.
[28] L. Zhang, Q. Feng, J. Wang, S. Zhang, B. Ding, Y. Wei, M. Dong, J.Y. Ryu, T.Y. Yoon, X. Shi, J. Sun, X. Jiang, Microfluidic synthesis of hybrid nanoparticles with controlled lipid layers: understanding flexibility-regulated cell-nanoparticle interaction, ACS Nano 9 (2015) 9912–9921.
[29] J. Sun, L. Zhang, J. Wang, Q. Feng, D. Liu, Q. Yin, D. Xu, Y. Wei, B. Ding, X. Shi, X. Jiang, Tunable rigidity of (polymeric core)-(lipid shell) nanoparticles for regulated cellular uptake, Adv. Mater. 27 (2015) 1402–1407.
[30] S. Zhang, H. Aslan, F. Besenbacher, M. Dong, Quantitative biomolecular imaging by dynamic nanomechanical mapping, Chem. Soc. Rev. 43 (2014) 7412–7429.
[31] P. Gentile, V. Chiono, I. Carmagnola, P.V. Hatton, An overview of poly(lactic-co-glycolic) acid (PLGA)-based biomaterials for bone tissue engineering, Int. J. Mol. Sci. 15 (2014) 3640–3659.
[32] Y. Takechi-Haraya, K. Sakai-Kato, Y. Abe, T. Kawanishi, H. Okuda, Y. Goda, Atomic force microscopic analysis of the effect of lipid composition on liposome membrane rigidity, Langmuir 32 (2016) 6074–6082.
[33] G. Hermann, P. Heffeter, T. Falta, W. Berger, S. Hann, G. Koellensperger, In vitro studies on cisplatin focusing on kinetic aspects of intracellular chemistry by LC-ICP-MS, Metallomics. 5 (2013) 636–647.
[34] H. Yin, R.L. Kanasty, A.A. Eltoukhy, A.J. Vegas, J.R. Dorkin, D.G. Anderson, Non-viral vectors for gene-based therapy, Nat. Rev. Genet. 15 (2014) 541–555.
[35] S.D. Conner, S.L. Schmid, Regulated portals of entry into the cell, Nature 422 (2003) 37–44.
[36] R.A. Petros, J.M. DeSimone, Strategies in the design of nanoparticles for therapeutic applications, Nat. Rev. Drug Discov. 9 (2010) 615–627.
[37] J. Gilleron, W. Querbes, A. Zeigerer, A. Borodovsky, G. Marsico, U. Schubert, K. Manygoats, S. Seifert, C. Andree, M. Stoter, H. Epstein-Barash, L. Zhang, V. Koteliansky, K. Fitzgerald, E. Fava, M. Bickle, Y. Kalaidzidis, A. Akinc, M. Maier, M. Zerial, Image-based analysis of lipid nanoparticle-mediated siRNA delivery, intracellular trafficking and endosomal escape, Nat. Biotechnol. 31 (2013) 638–646.
[38] T.G. Iversen, T. Skotland, K. Sandvig, Endocytosis and intracellular transport of nanoparticles: present knowledge and need for future studies, Nano Today 6 (2011) 176–185.
[39] R. Ursic-Bedoya, C.E. Mire, M. Robbins, J.B. Geisbert, A. Judge, I. MacLachlan, T.W. Geisbert, Protection against lethal Marburg virus infection mediated by lipid encapsulated small interfering RNA, J. Infect. Dis. 209 (2014) 562–570.
[40] K. Hollo, T.T. Glant, M. Garzo, A. Finnegan, K. Mikecz, E. Buzas, Complex pattern of Th1 and Th2 activation with a preferential increase of autoreactive Th1 cells in BALB/c mice with proteoglycan (aggrecan)-induced arthritis, Clin. Exp. Immunol. 120 (2000) 167–173.
[41] C. Kaplan, J.C. Valdez, R. Chandrasekaran, H. Eibel, K. Mikecz, T.T. Glant, A. Finnegan, Th1 and Th2 cytokines regulate proteoglycan-specific autoantibody isotypes and arthritis, Arthritis Res. 4 (2002) 54–58.